Formation and relaxation of rovibrationally excited H_2 molecules due to plasma-surface interaction

O. Gabriel, D. C. Schram, and R. Engeln*

Department of Applied Physics, Eindhoven University of Technology, P.O. Box 513, 5600 MB Eindhoven, The Netherlands

(Received 20 April 2008; published 29 July 2008)

We report on the interaction of hydrogen atoms and molecules under high flux conditions with a cooled copper surface and its impact on gas phase densities and internal excitation of the molecules. These densities were measured by means of laser-induced fluorescence using tunable radiation sources in the vacuum-ultraviolet (vuv). While H atoms were detected by two-photon absorption laser-induced fluorescence, the necessary vuv radiation for the detection of rovibrationally excited H_2 molecules in the electronic ground state were produced by stimulated anti-Stokes Raman scattering. The results reveal a strong loss mechanism of H atoms and the formation of rovibrationally excited H_2 molecules due to surface interaction. The surface reaction probability of H atoms under high flux conditions on copper was estimated. Surface collisions are shown to have a profound influence on the density distribution of rovibrationally excited H_2 molecules: The distributions follow lower temperatures and are less Boltzmann-like, i.e., the distributions of the internal excitation of H_2 molecules differ more from thermodynamic equilibrium.

DOI: 10.1103/PhysRevE.78.016407 PACS number(s): 52.40.Hf, 52.70.Kz, 34.50.Ez

I. INTRODUCTION

Hydrogen will play a vital role in future technologies ensuring our energy supply and reducing our dependence on limited fossil fuels. Used as an energy storage medium, it will be part of the so-called hydrogen economy [1]. In future nuclear fusion reactors hydrogen isotopes deuterium and tritium will be used as fuel [2]. However, the control of the interaction between plasma gas phase and surrounding surfaces in a fusion reactor is a challenging and until now unsolved technological task [3]. While hydrogen is fully dissociated and ionized in the core of a fusion plasma, hydrogen molecules were detected in the cooler parts close to reactor surfaces, such as the divertor region. These molecules are formed in rovibrationally excited states by association processes at surfaces [4–8] and can influence the condition and the stability of a fusion plasma [9,10].

Hydrogen containing plasmas are also widely used in applications such as the deposition of ultrahard diamondlike films or amorphous-microcrystalline silicon layers in solar cell production [11–13]. Hydrogen atoms are important for the formation of deposition precursors from injected monomers (e.g., SiH_3 from SiH_4) within the plasma gas phase, while on plasma facing surfaces hydrogen determines the surface chemistry, e.g., crystallization processes resulting in the formation of diamondlike structures [14].

Important parameters for plasma gas phase characterization are the densities of reactive species, such as ions and radicals, and their energies. These energies are kinetic energies as well as energies due to internal excitation. The internal excitation can be electronically, and, in case of molecules, due to vibration and rotation. Although the influence of rovibrationally excited molecules on the plasma gas phase and surface chemistry has been predicted, it is still a rather unexplored research field. For example, inelastic electron collisions are substantially enhanced if the molecules are rovibrationally excited [15]. Until now, descriptions and computational simulations of molecular plasmas often include a vibrational excitation, but usually neglect a rotational excitation of molecules [16].

However, it is well known that reaction rates depend on the total internal energy, i.e., on the vibrational state v as well as the rotational state J of a molecule [17]. For instance, the rate coefficients for dissociative attachment of H_2 by inelastic electron collisions ($H_2+e\rightarrow H^-+H$) are enhanced for vibrationally excited H_2 [18–21]. On the other hand, recent reports have revealed that dissociative attachment cross sections are enhanced by several orders of magnitude, if H_2 is in a rotationally excited state $(v,J)=(0,30)$ compared to the rovibrational ground state (0,0) [22]. Therefore, this enhancement by rotational excitation is of great relevance for the H_2 plasma chemistry.

Both, laboratory experiments and computational simulations, have demonstrated that hydrogen molecules can be formed by surface association processes, and that the released H_2 molecules are rovibrationally excited [23–27]. The excitation level of the product depends on the surface material and temperature. The products can be highly rotationally excited, while the distribution of their internal energies is far away from thermodynamic equilibrium [28].

Furthermore, surface interaction of hydrogen containing plasmas is a more general phenomenon. While the flux of hydrogen atoms and ions towards surfaces is very large in fusion experiments (10^{22}–10^{24} m^{-2} s^{-1}), the other extreme of the scale are very low flow conditions in interstellar media. There, molecules are formed by surface association on cold dust grains [29–31]. The interaction of hydrogen atoms with these surfaces is the dominant molecule formation process, where gas phase reactions play only a minor role due to low densities and low gas phase recombination cross sections. The flux conditions in our experiments are between these two extremes, i.e., a few orders lower than in fusion experiments, but still high compared to other experiments.

*r.engeln@tue.nl

A common way to measure excited H_2 molecules is optical emission spectroscopy on the H_2 Fulcher band [5–8,32,33]. However, detailed knowledge of the excitation mechanisms is necessary to obtain electronic ground state ($X\,^1\Sigma_g^+$) densities. Direct spectroscopic detection of H_2 molecules in the $X\,^1\Sigma_g^+$ state is challenging, because transitions within this state are dipole forbidden and the energy gap to the first excited electronic state $B\,^1\Sigma_u^+$ is large ($\approx$10 eV), i.e., these so-called Lyman transitions occur in the vacuum ultraviolet (vuv) spectral range. Various tunable vuv sources have been applied to $H_2(v,J)$ detection [34–37]. Lower rovibrational states ($v \leqslant 2$) are detectable by means of coherent anti-Stokes Raman spectroscopy (CARS) [38–42], while stimulated anti-Stokes Raman scattering (SARS) has been applied successfully for the detection of higher rovibrational states with excellent sensivity [43–48].

In this paper we report on the influence of surface collisions in a cascaded arc, i.e., in a thermal plasma source, on the distributions of rovibrationally excited H_2 molecules. An effect on the formation of rovibrationally excited H_2 in its electronic ground state is revealed by exposing surfaces to plasma under high flow conditions towards cooled copper surfaces with different areas. While the internal energy distributions of H_2 molecules are measured by means of SARS, additional measurements of the H atom densities by two-photon absorption laser-induced fluorescence (TALIF) indicate a fast formation of H_2 molecules by surface association.

II. EXPERIMENT

The plasma source has been described in detail elsewhere [49,50], and only a brief description is given here. Hydrogen gas flows with a flow rate of 3000 sccm (1.25×10^{21} s^{-1}) under subatmospheric pressure of about 9 kPa into the plasma source, a wall-stabilized cascaded arc. The arc channel is 4 cm long with a diameter of 4 mm (see Fig. 1). A partially ionized and dissociated hydrogen plasma is produced in the channel driven by a current of 60 A and a power input of 9 kW. Cascade and anode plates are made from copper and are water cooled. The plasma expands at the exit of the channel through a copper nozzle supersonically into a vacuum chamber (2 m long and 0.3 m in diameter), where pumps keep the pressure at 100 Pa. These conditions lead to a sonic exit velocity of about $c_0=\sqrt{\gamma k_B T_{\mathrm{exit}}/m} \approx 5000$ m/s (γ, adiabatic index and/or heat capacity ratio; k_B, Boltzmann constant; T_{exit}, exit temperature; m, mass), a value confirmed in earlier experiments [51]. A shock front is formed downstream of the nozzle, where the plasma expansion undergoes a transition to subsonic flow [50].

State selective detection of rovibrationally excited hydrogen molecules is performed by means of laser-induced fluorescence (LIF) in the vuv. The vuv radiation is produced by stimulated anti-Stokes Raman scattering (SARS) [43–48]. A scheme of the beam path and the spectroscopic setup is shown in Fig. 2. Tunable laser radiation in a wavelength range from 436 nm to 470 nm is provided by a dye laser that is pumped by a frequency tripled Nd:YAG laser. The dye laser radiation is frequency doubled in a beta barium borate crystal resulting in pulses of 5 ns duration and with energies

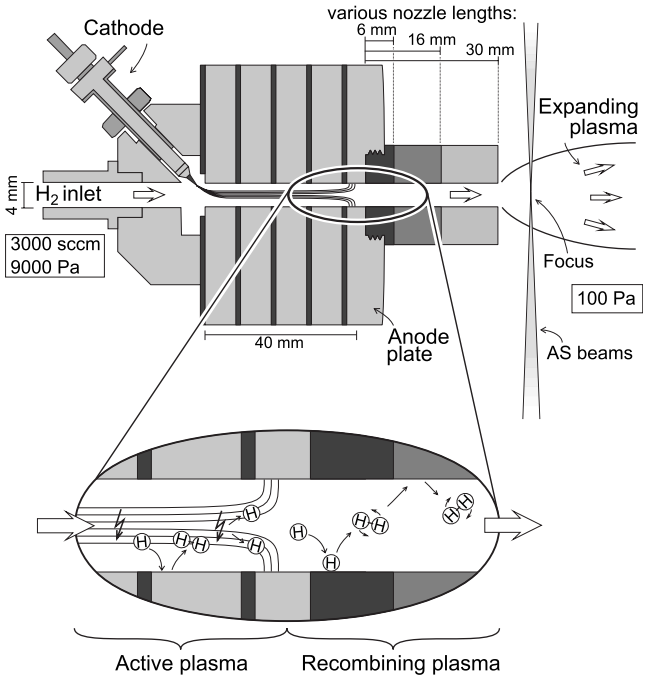

FIG. 1. The plasma source, a cascaded arc, operated with nozzles of three different lengths. At the bottom is shown a scheme of the assumed processes within arc channel and nozzles.

of 5–10 mJ in the spectral range from 218 nm to 235 nm and a bandwidth of 0.15 cm^{-1}. This beam is focused into a Raman cell, filled with 250 kPa of hydrogen gas cooled by liquid nitrogen to enhance the SARS process. The high laser intensity in the focus enables the SARS process, which produces laser-like coherent Stokes (S) and anti-Stokes (AS) beams. The AS beams are subsequently shifted to higher frequencies by the vibrational Raman shift of H_2, i.e.,

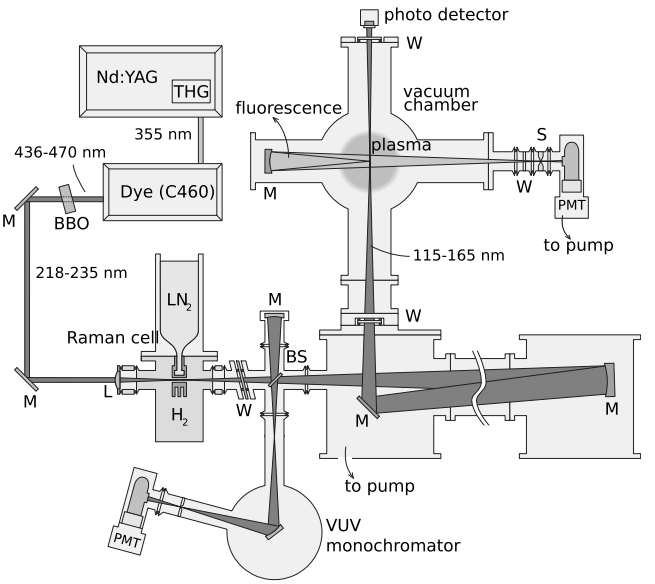

FIG. 2. The setup with the laser and anti-Stokes beam paths within the vuv spectrometer and the vacuum chamber (M, mirror; L, lens; BS, beam splitter; W, MgF_2 window; S, slit; PMT, photomultiplier tube).

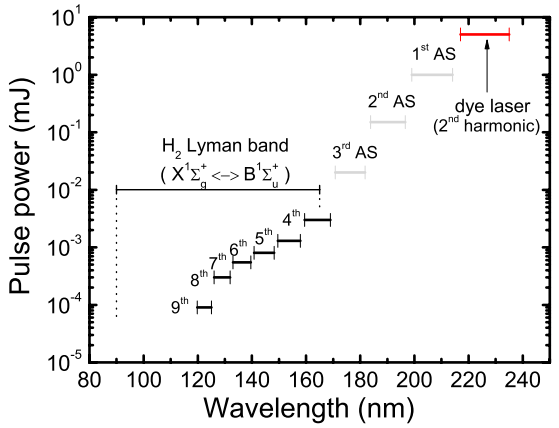

FIG. 3. (Color online) Wavelength and pulse energy distribution of the anti-Stokes beams produced in the Raman cell. Also shown is the spectral range of the H_2 Lyman band.

4155.22 cm^{-1}. Each AS beam is subsequently reduced in pulse energy due to the nonlinear stimulated Raman process (see Fig. 3). Thereby, the fourth through ninth AS cover a range from 115 nm to 165 nm, i.e., about 2/3 of the spectral range of the H_2 Lyman band. The wavelength range lower than 110–115 nm is prohibited by the nonavailability of vuv transparent windows.

All Raman orders together are focused by vuv optics into the center of the vacuum chamber. Hence, the excitation of H_2 in the plasma jet happens simultaneously at several AS frequencies. The fluorescence signal ($B\ ^1\Sigma_u^+ \rightarrow X\ ^1\Sigma_g^+$) of excited H_2 molecules is collected by a mirror perpendicular to the AS beams and the plasma expansion and then focused into a photomultiplier tube. Therefore, a measured spectrum is a superposition of multiple spectra, each caused by one of the AS beams, a process called multiplexed LIF. The disadvantage of a more complicated spectrum is compensated by the time saving of multiplexing. Spectra analysis is performed using spectroscopic data for the H_2 Lyman band provided by Abgrall *et al.* [52,53]. A fluorescence yield is calculated for each detected transition using a radiative model including the excitation rate, spontaneous and stimulated emission probabilities, and taking into account saturation effects. Depending on the fluorescence yield, the minimal detectable H_2 state density is about 10^{13} m^{-3}.

H atom densities are measured by two-photon absorption laser-induced fluorescence (TALIF). Therefore, the dye laser is pumped by a frequency doubled Nd:YAG laser and the resulting dye laser radiation (around 615 nm) is tripled by KDP and BBO crystals to 205 nm. The laser beam is focused perpendicular to the plasma expansion into the center of the vacuum chamber. Hydrogen ground-state atoms are excited by two photons to the $3s^2D$ and $3s^2S$ states (L_β) and the resulting fluorescence (H_α) is measured by a photomultiplier tube. Absolute densities are obtained by calibration using a two-photon transition in a known amount of krypton [54].

In order to study the interaction of H atoms and H_2 molecules with a copper surface, nozzles of this material and of various lengths (6 mm, 16 mm, 28 mm) are mounted to the anode plate in the experiments, see Fig. 1. By changing the nozzle length, also the nozzle surface area changes, which is in contact with the plasma after it left the arc channel. The AS beam focus as well as the laser focus for TALIF are positioned in the center of the expanding plasma jet 8 mm downstream of the nozzle exit, but still before the position z_M of the expansion shock front, which is given by

$$z_M = 0.02 \sqrt{\frac{\Phi}{p_{\text{back}}} \sqrt{T_{\text{exit}} A}} \quad \text{(in m)} \tag{1}$$

with the gas flow Φ in sccs (standard cubic centimeter per second), background pressure p_{back} in Pa, the mass A in amu, and the exit temperature T_{exit} in eV [55]. The exit temperature, as it will be shown later, depends on the nozzle length, and varies from 0.36 eV to 0.42 eV resulting for our conditions in shock positions between 13.0 mm and 13.5 mm. Therefore, all measurements are performed within the supersonic plasma expansion.

III. MEASURED AND SIMULATED H_2 DENSITY DISTRIBUTIONS

State densities of rovibrationally excited H_2 molecules measured with nozzles of three different lengths are shown in Fig. 4. The lines in the figures represent a model for the $H_2(v,J)$ distribution that was used in the spectra calculation and that was fitted to the measured spectra. The points in the figures represent densities obtained from the integrated area under pronounced peaks in the measured spectra.

The model for the H_2 density distribution is a superposition of two different Boltzmann distributions of the rovibrational states. Lower rotational states ($J<7$) of each vibrational state follow a Boltzmann distribution described by a temperature of 700 K, i.e., close to the temperature of the gas in the background of the vacuum chamber. On the other hand, the higher rotational states follow a Boltzmann-like distribution with a much higher temperature between 2900 K and 4500 K. The distribution of the vibrational states can also be described by this temperature. Therefore, we will call this temperature T_{vib}, although one should be aware of the fact that the term "temperature" may be inappropriate in case of non-Boltzmann distributions. Similar distributions were measured also by others and in other types of hydrogen discharges (see [56–58], and references therein). A special case is the first vibrational state ($v=0$), for which the first rotational states have been reported in [41] to have a factor of 20 higher densities than expected from the trend in the higher vibrational states. This is probably due to mixing of the hot gas from the plasma source with the cool background gas, which populates the first rotational states of the $v=0$ state.

We want to emphasize the high rotational excitation we found for some of the excited H_2 molecules. Rotational excitation levels higher than $J=20$ were found in case of the short nozzles (6 mm and 16 mm), while for the long nozzle (30 mm) the densities of higher rovibrationally excited H_2 molecules were below the detection limit. The highest rovibrational excitations are only a few 0.1 eV below the dissociation limit at 4.5 eV.

While the SARS technique results in relative values for the density distribution of internal H_2 states, absolute H_2

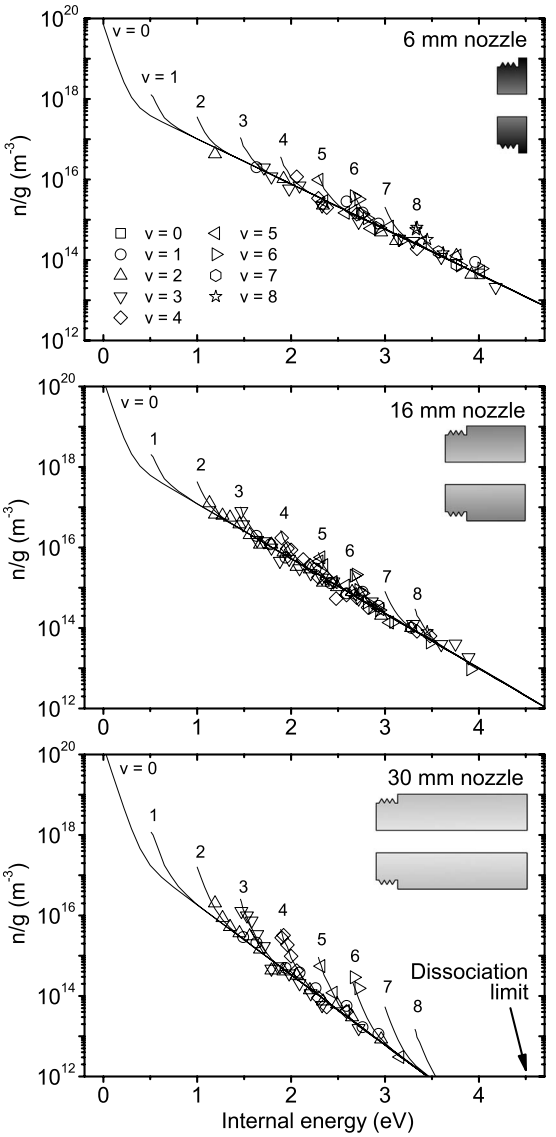

FIG. 4. Distributions of the total internal energy of rovibrationally excited H_2 molecules measured with nozzles of three different lengths. The lines represent the fits, while the symbols are obtained from measured peaks in the spectra. Densities are plotted logarithmically and per statistical weight g (Boltzmann plot).

state densities are derived by comparison with the total H_2 density measured by means of Rayleigh scattering in a previous work [59]. By using a 16 mm long nozzle and the same process conditions as in the present work, the H_2 density was found to be 3.0×10^{21} m^{-3} at a position 8 mm in front of the nozzle exit. For the nozzles with lengths of 6 mm and 30 mm the total H_2 densities were derived by comparison with this reference point. This results in total H_2 densities of 1.5×10^{21} m^{-3} and 3.0×10^{21} m^{-3} for the 6 mm and the 30 mm nozzle, respectively. The relative error of these densities is in the order of 50% due to power fluctuations of the AS beams.

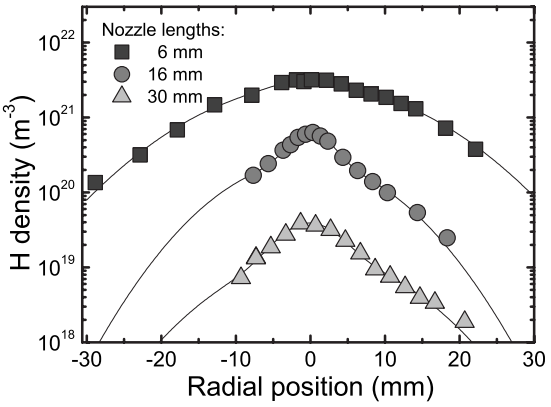

FIG. 5. Radial scans of the H atom densities 8 mm in front of the nozzle exit for three different nozzle lengths.

IV. MEASURED H ATOM DENSITIES

H atom densities measured by means of TALIF at the same position in the plasma jet are shown in Fig. 5. These values are in agreement with previous measurements performed with nozzle lengths of 6 mm and 16 mm [60], while we give here an additional result for the 30 mm nozzle. The values are summarized in Table I. Also given in the table are the total densities in the jet. Since the densities of ions, electrons, and electronically excited H atoms and H_2 molecules are orders of magnitude lower than ground-state atom and molecule densities, we neglect these species.

The dissociation degree, $n_H/(n_H+2n_{H_2})$, was calculated for all three experiments (see Table I). Using the short nozzle (6 mm) the dissociation degree is around 50%, a value close to the dissociation degree inside the arc channel [41]. With the 16 mm nozzle we obtain a value of 10%, that was reported also in [59]. On the other hand, using the longest nozzle of 30 mm length, the dissociation degree is less than 1%. This clearly indicates a strong loss mechanism of H atoms inside the nozzle channel (see Sec. VI).

V. TEMPERATURES INSIDE THE NOZZLE AND IN THE PLASMA EXPANSION

The kinetic gas temperatures have been calculated from the linewidths of the measured H_2 (vuv-LIF) and H (TALIF)

TABLE I. Summary of H_2 and H densities measured 8 mm in front of the nozzle and the corresponding dissociation degree.

Nozzle length	Total density (m^{-3})	H_2 density (m^{-3})	H density (m^{-3})	Dissociation degree (%)
6 mm	4.7×10^{21}	1.5×10^{21}	3.2×10^{21}	51.6
16 mm	3.6×10^{21}	3.0×10^{21}	6.2×10^{20}	9.4
30 mm	3.0×10^{21}	3.0×10^{21}	4.3×10^{19}	0.6

TABLE II. Vibrational and kinetic temperatures of H_2 and H measured 8 mm in front of the nozzles.

Nozzle length	H_2 molecules		H atoms
	T_{vib} (K)	T_{kin} (K)	T_{kin} (K)
6 mm	4500 ± 200	1200 ± 500	1400 ± 300
16 mm	3700 ± 200	900 ± 150	1050 ± 300
30 mm	2900 ± 200	600 ± 200	900 ± 300

line profiles. They are listed for the axial position $z=8$ mm in Table II together with the vibrational H_2 temperatures at the same position derived from the distributions in Fig. 4. While T_{kin} is comparable for both, H_2 molecules and H atoms, the values for T_{vib} of H_2 are about 4 times higher. Therefore, the plasma is far off from thermodynamic equilibrium. There are much more high rovibrationally excited H_2 molecules as one would expect from the kinetic temperature, indicating a strong production of these high excited molecules, e.g., due to surface association processes. However, the kinetic temperature is determined due to the Doppler shift in the direction of the laser beam path. Therefore, we measured the kinetic temperatures perpendicular to the direction of the expansion. It is well known from earlier measurements [61,62] and theory [63] that the parallel temperature stays constant at a value higher than the perpendicular temperature, while the perpendicular temperature decays in the expansion due to adiabatic cooling.

Apparently, the kinetic temperature as well as the vibrational temperature decay with increasing nozzle length due to a heat flow from the plasma towards the water cooled nozzles. Since densities and temperatures were measured downstream of the nozzles at $z=8$ mm, the question arises, whether this also gives information about the conditions and developments inside the nozzles. We calculated the temperature at the nozzle exit using the well-known temperature development at the center axis of an expanding hot gas and/or plasma,

$$T(z) = \frac{T_{exit}}{(1 + z^2/z_0^2)^{\gamma-1}}, \tag{2}$$

where γ is the adiabatic index (heat capacity ratio), z is the distance from the nozzle, and z_0 is introduced to take into account that the expansion starts already inside the nozzle, i.e., slightly before the nozzle exit. For a straight nozzle, z_0 is in the order of the nozzle radius (here, 2 mm). The adiabatic index γ would be 1.3 for a pure molecular H_2 gas at these temperatures, but we use 1.7, a value that was found for H_2/H containing hydrogen hot plasma expansions in [51].

With Eq. (2) the exit temperatures were found to be 4700 K, 3650 K, and 2450 K for the 6 mm, 16 mm, and 30 mm nozzle length, respectively. These values are very close to the vibrational temperatures of the molecules (see Table II), which indicates that T_{kin} and T_{vib} are in equilibrium, if we assume that the vibrational temperature does not change between the nozzle exit and $z=8$ mm in the expansion. Such a relaxation behavior of rovibrationally excited H_2 molecules was investigated previously [57]. It was found that the decay rate of a rotational state increases with the rotational number until $J=7$, but stays constant for higher rotational states [57]. Therefore, the vibrational temperature "freezes" and stays constant during the gas phase expansion.

On the other hand, the vibrational temperatures, given by the distributions in Fig. 4, decrease with increasing nozzle lengths. The hydrogen plasma is not only cooled inside the nozzles, but the shapes of the distributions change and become more non-Boltzmann-like with increasing nozzle length. The higher rotational states ($J>6$) are faster depopulated than the lower states.

Within the gas phase only molecule-molecule and, less important due to lower atom densities, molecule-atom collisions contribute to the redistribution of the internal energies of H_2 molecules [41,57,64,65]. The situation inside the nozzles is different. There, the internal energies of H_2 are redistributed not only by gas phase reactions and collisions, but also by molecule-surface collisions and the production of rovibrationally excited H_2 due to surface association [25–27]. Wall cooling was also found to be the dominant cooling mechanism in a recombining plasma [66], as well as for rovibrationally excited H_2 produced on a heated filament [42]. In [67] it was shown that by surface collisions an internal (rotational) energy of H_2 can be converted even into translational energy. However, the exact nature of the cooling processes inside the nozzles remains unknown and further investigations are necessary.

For a description of the processes inside the nozzles we need to know the development of the temperature. We assume that the temperature inside the nozzles follow an exponential decay,

$$T(z) = T_0 e^{-z/z_{temp}}, \tag{3}$$

where T_0 is the temperature at the end of the arc and z_{temp} is the distance at which the temperature declines by $1/e$. Both parameters are assumed to be the constant for all three types of nozzles. Their values were fitted to match the values for the temperatures at the nozzle exits and result in $T_0 = 5500$ K (0.45 eV) and $z_{temp}=37$ mm.

The resulting temperature developments inside and outside the nozzles are shown in Fig. 6. The exit temperature depends on the nozzle length and influences the exit velocity $c_0=\sqrt{\gamma k_B T_{exit}/m}$, which is 5700 m/s for the 6 mm nozzle, 5000 m/s for the 16 mm nozzle, and 4100 m/s for the 30 mm nozzle.

VI. SURFACE ASSOCIATION AT THE NOZZLE SURFACE

The loss of hydrogen atoms inside the nozzle depends on the nozzle length as shown in Table I. Several possible mechanisms for the loss of H atoms inside the nozzle are discussed in [60]. Volume loss due to three-body recombination of H atoms is very unlikely under our conditions, since its time constant is around 2 ms inside the arc channel, because the maximal densities are in the order of 10^{23} m^{-3} and the rate coefficient is 5×10^{-44} $m^6 s^{-1}$ [60]. On the other hand, flow velocities around 5000 m/s result in a residence time of only 2 μs in a nozzle of 10 mm length.

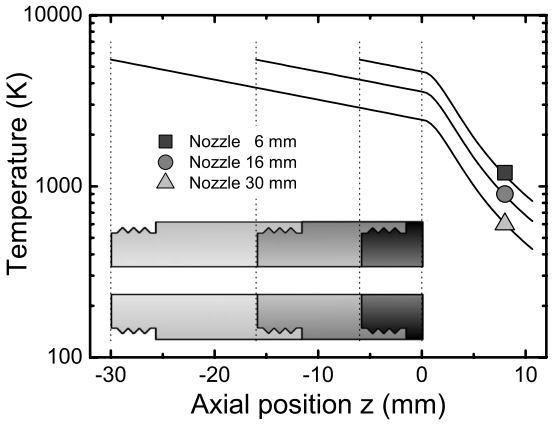

FIG. 6. Measured H_2 temperatures at $z=8$ mm compared to calculated temperature developments inside and outside of the three nozzles.

Surface association of H atoms forming H_2 molecules is supposed to be the most probable process. Similar to the discussion of the temperature development in Sec. V the density n_{exit} of H atoms at the nozzle exit was calculated using the known decay in the plasma expansion [55,68],

$$n(z) = \frac{n_{exit} z_0^2}{z^2 + z_0^2}, \tag{4}$$

where z_0 is again in the order of the nozzle radius, see Eq. (2). The resulting H densities at the nozzle exits are summarized in Table III.

In a next step we will give an estimate of the surface reaction probability of H atoms on the nozzle surface, i.e., the cooled copper material. Therefore, we assume a viscous flow, which is reasonable since the mean free path λ_{mfp} is two orders of magnitude lower than the nozzle dimensions (4 mm) under our conditions. The mean free path is calculated using a hard sphere model with an effective collision area of 3×10^{-19} m^2 [69] and a typical density of 10^{23} m^{-3}. This results in $\lambda_{mfp}=0.03$ mm.

The loss of H atoms due to diffusion of H atoms towards the surface of the nozzle and with a surface reaction probability α is given for a cylindrical geometry by

$$\frac{1}{k_{wall}} = \tau = \frac{\Lambda_0^2}{D} + \frac{V}{A}\frac{2(2-\alpha)}{\bar{v}\alpha}, \tag{5}$$

where Λ_0 is the diffusion length, D is the diffusion coefficient, $\bar{v}$ is the mean kinetic velocity, τ is the lifetime of H atoms, and V/A is the volume-to-surface area ratio [70,71].

TABLE III. Temperatures and H and H_2 densities at the nozzle exits.

Nozzle length	T_{exit} (K)	$[H]_{exit}$ (m^{-3})	$[H_2]_{exit}$ (m^{-3})
6 mm	4700	3.3×10^{22}	2.9×10^{22}
16 mm	3650	9.5×10^{21}	7.2×10^{22}
30 mm	2450	5.8×10^{20}	1.3×10^{23}

The diffusion lengths Λ_0 for the three different nozzles are 7.6×10^{-4} m (6 mm nozzle), 8.2×10^{-4} m (16 mm nozzle) and 8.3×10^{-4} m (30 mm nozzle), again assuming a cylinder [70]. The diffusion coefficient is $D=\frac{2}{3}\bar{v}\lambda_{mfp}=0.3$ m^2 s^{-1}, while the mean kinetic velocity is $\bar{v}=\sqrt{\frac{3k_BT}{m}}\approx10^4$ m/s, and V/A is 10^{-3} m for all three nozzles.

Hydrogen molecules and atoms are the dominating species inside the nozzles, since ions can usually be neglected due to the low ionization degree, which is orders of magnitude lower than the dissociation degree. The total density is therefore given by $n_{H2}+n_H$. With an assumed linear pressure drop within arc and nozzles (from 10 kPa to a few kPa) and the temperature decay presented in Sec. V, the total density is nearly constant at $1.0\pm0.3\times10^{23}$ m^{-3}.

The development of λ_{mfp}, D and $\bar{v}$, and thus with Eq. (5) the loss rate k_{wall} of hydrogen atoms, were calculated at each position within the nozzles. While pressure and temperature determine the total density at each position, the H atom loss rate k_{wall} changes the ratio between n_{H2} and n_H. Here, we assume that the surface reaction probability α in Eq. (5) lead to a loss of H atoms and the formation of H_2 by surface association. Surface sticking, reflection, and desorption of H atoms are neglected, because these mechanisms do not change the H density within the nozzles under steady-state conditions.

Free parameters in this simple model are the dissociation degree in the arc, i.e., the values of n_{H2} and n_H at the start of the nozzles, and the surface reaction probability α. We found that only a dissociation degree of 0.99 (almost fully dissociated hydrogen plasma) and a surface reaction probability of $\alpha=0.32$ lead to H and H_2 densities as they are summarized in Table III. The resulting developments of the H and H_2 densities inside and outside the nozzles are shown in Fig. 7.

Although we found strong losses of H atoms inside the nozzles due to surface association, the predicted formation of high rovibrationally excited H_2 molecules [25–27] is not visible in the distributions shown in Fig. 4. The reason is the redistribution of the internal energy of H_2 due to molecule collisions with the cooled copper surface of the nozzles and molecule-molecule collisions within the gas phase. Therefore, the decay of the vibrational and rotational temperatures is stronger than the production of high rovibrationally excited H_2, and thus this production is not directly measurable.

The measured H and H_2 densities are reproduced well in the model with a mean relative error of 24%. The main contribution to this error is the difference in the density of H_2 for the 30 mm nozzle, which is probably due to the rather large relative error of the H_2 densities measured by SARS. Without this data point the relative error is only 13%. We also calculated the dependence of this relative error on the fit parameters α and the dissociation degree. The result is shown in Fig. 8. Clearly visible are the minima at the mentioned values.

The value for α is in the same order of magnitude found by others, which is e.g., 0.5 for H/D association on Cu(111) surfaces [25]. However, these experiments were performed with low atomic fluxes on a cleaned and well-defined Cu surface that was cooled to 100 K and was fully covered with H/D atoms. On the other hand, the surface inside the nozzle

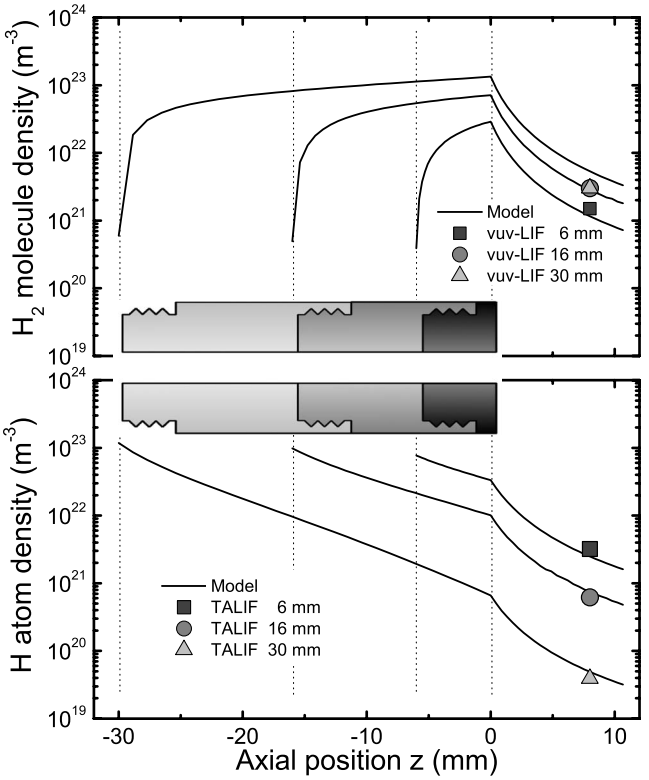

FIG. 7. The development of the H_2 molecule (top) and H atom densities (bottom) within and outside the three nozzles. The curves within the nozzle are calculated using a surface association model, while the decay outside follow the $1/z^2$ dependence of expanding gases and/or plasma described by Eq. (4).

in our experiments is much hotter and exposed to an enormous heat flux and particle flow. In this respect, the similarity in the results is astonishing.

VII. CONCLUSIONS

Distributions of the internal energy of rovibrationally excited H_2 molecules have been measured by vuv-LIF in an expanding thermal H_2 plasma, using stimulated anti-Stokes Raman scattering (SARS) for the production of the vuv radiation. The $H_2(v,J)$ distributions differ from a Boltzmann distribution and depend strongly on the exposure time of the

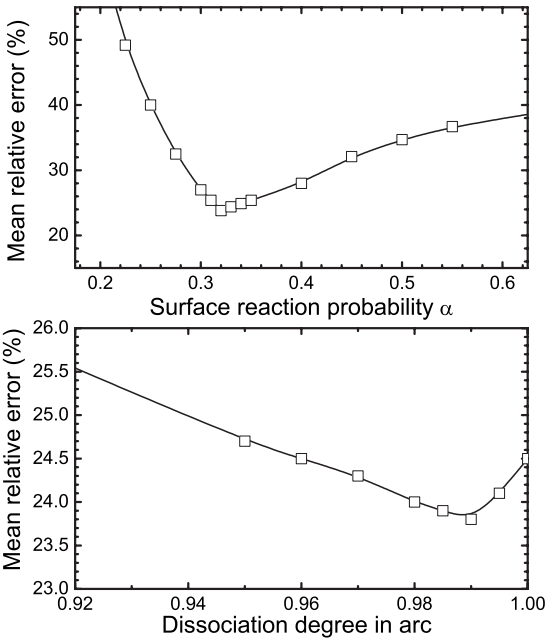

FIG. 8. The mean relative error of the surface association model depending on the surface reaction probability (top) and the dissociation degree in the arc (bottom).

hot gas to a cooled copper surface. The relaxation of excited H_2 molecules due to surface collisions is faster than the relaxation in the gas phase found in earlier experiments. The temperatures are the lower the longer the gas-surface interaction lasts. TALIF measurements of H atom densities using nozzles of various lengths reveal a strong H atom loss depending on the surface exposure time inside the nozzles, in agreement with increasing H_2 densities. A high surface association rate was found for H atoms on cooled copper surfaces. The association rate is close to values found by others, although our copper surfaces were much hotter.

ACKNOWLEDGMENTS

This work is part of the research program of the Dutch Foundation for Fundamental Research on Matter (FOM). The work is also supported by the Euratom Foundation. We greatly appreciate the skillful technical assistance of M. J. F. van de Sande, J. J. A. Zeebregts, J. F. C. Jansen, and H. M. M. de Jong.

[1] L. Schlapbach and A. Züttel, Nature (London) **414**, 353 (2001).
[2] U. Samm, Contemp. Phys. **44**, 203 (2003).
[3] A. W. Kleyn, W. Koppers, and N. Lopes Cardozo, Vacuum **80**, 1098 (2006).
[4] J. Wesson, *Tokamak* (Clarendon, Oxford, 1997).
[5] U. Fantz, D. Reiter, B. Heger, and D. Coster, J. Nucl. Mater. **290-293**, 367 (2001).
[6] S. Brezinsek, P. Mertens, A. Pospieszczyk, G. Sergienko, and P. T. Greenland, Contrib. Plasma Phys. **42**, 668 (2002).
[7] H. Kubo, H. Takenaga, K. Sawada, T. Nakano, S. Kobayashi, S. Higashijima, N. Asakura, and K. Shimizu, J. Nucl. Mater. **337-339**, 161 (2005).
[8] A. Pospieszczyk, S. Brezinsek, G. Sergienko, P. T. Greenland, A. Huber, A. Meigs, P. Mertens, U. Samm, M. Stamp, and S. Wiese, J. Nucl. Mater. **337-339**, 500 (2005).
[9] J. Winter, Plasma Phys. Controlled Fusion **38**, 1503 (1996).
[10] U. Samm and the TEXTOR-94 Team, Plasma Phys. Controlled Fusion **41**, B57 (1999).
[11] T. Ohira, O. Ukai, and M. Noda, Surf. Sci. **458**, 216 (2000).

[12] M. N. van den Donker, B. Rech, F. Finger, W. M. M. Kessels, and M. C. M. van de Sanden, Appl. Phys. Lett. **87**, 263503 (2005).
[13] W. M. M. Kessels, K. Nadir, and M. C. M. van de Sanden, J. Appl. Phys. **99**, 076110 (2006).
[14] J. C. Angus and C. C. Hayman, Science **241**, 913 (1988).
[15] R. Celiberto, R. K. Janev, A. Laricchiuta, M. Capitelli, J. M. Wadehra, and D. E. Atems, At. Data Nucl. Data Tables **77**, 161 (2001).
[16] U. Fantz and P. T. Greenland, Contrib. Plasma Phys. **42**, 694 (2002).
[17] R. D. Levine, Annu. Rev. Phys. Chem. **29**, 59 (1978).
[18] M. Allan and S. F. Wong, Phys. Rev. Lett. **41**, 1791 (1978).
[19] J. R. Hiskes, A. M. Karo, and P. A. Willmann, J. Appl. Phys. **58**, 1759 (1985).
[20] C. Gorse, M. Capitelli, J. Bretagne, and M. Bacal, Chem. Phys. **93**, 1 (1985).
[21] T. Mosbach, Plasma Sources Sci. Technol. **4**, 610 (2005).
[22] J. Horáček, M. Čížek, K. Houfek, P. Kolorenč, and W. Domcke, Phys. Rev. A **70**, 052712 (2004).
[23] R. I. Hall, I. Cadez, M. Landau, F. Pichou, and C. Schermann, Phys. Rev. Lett. **60**, 337 (1988).
[24] P. J. Eenshuistra, R. M. A. Heeren, A. W. Kleyn, and H. J. Hopman, Phys. Rev. A **40**, 3613 (1989).
[25] C. T. Rettner and D. J. Auerbach, J. Chem. Phys. **104**, 2732 (1996).
[26] B. Jackson and D. Lemoine, J. Chem. Phys. **114**, 474 (2001).
[27] T. Zecho, A. Güttler, X. Sha, B. Jackson, and J. Küppers, J. Chem. Phys. **117**, 8486 (2002).
[28] A. J. H. M. Meijer, A. J. Farebrother, and D. C. Clary, J. Phys. Chem. A **106**, 8996 (2002).
[29] L. Hornekær, A. Baurichter, V. V. Petrunin, D. Field, and A. C. Luntz, Science **302**, 1943 (2003).
[30] S. Cazaux and A. G. G. M. Tielens, Astrophys. J. **604**, 222 (2004).
[31] S. C. Creighan, J. S. A. Perry, and S. D. Price, J. Chem. Phys. **124**, 114701 (2006).
[32] B. P. Lavrov, A. S. Melnikov, M. Käning, and J. Röpcke, Phys. Rev. E **59**, 3526 (1999).
[33] B. Xiao, S. Kado, S. Kajita, and D. Yamasaki, Plasma Phys. Controlled Fusion **46**, 653 (2004).
[34] E. E. Marinero, C. T. Rettner, and R. N. Zare, Chem. Phys. Lett. **95**, 486 (1983).
[35] F. J. Northrup, J. C. Polanyi, S. C. Wallace, and J. M. Williamson, Chem. Phys. Lett. **105**, 34 (1984).
[36] W. Meier, G. Ahlers, and H. Zacharias, J. Chem. Phys. **85**, 2599 (1986).
[37] C. D. Pibel, K. L. Carleton, and C. B. Moore, J. Chem. Phys. **93**, 323 (1990).
[38] M. Péalat, J. P. E. Taran, J. Taillet, M. Bacal, and A. M. Bruneteau, J. Appl. Phys. **52**, 2687 (1981).
[39] M. Péalat and J.-P. E. Taran, J. Chem. Phys. **82**, 4943 (1985).
[40] G. J. Germann and J. J. Valentini, J. Phys. Chem. **92**, 3792 (1988).
[41] R. F. G. Meulenbroeks, R. A. H. Engeln, J. A. M. van der Mullen, and D. C. Schram, Phys. Rev. E **53**, 5207 (1996).
[42] H. Umemoto, S. Ansari, and H. Matsumara, J. Appl. Phys. **99**, 043510 (2006).
[43] D. J. Brink and D. Proch, Opt. Lett. **7**, 494 (1982).
[44] M. Spaan, A. Goehlich, V. Schultz-von der Gathen, and H. F. Döbele, Appl. Opt. **33**, 3865 (1994).
[45] H. F. Döbele, Plasma Sources Sci. Technol. **4**, 224 (1995).
[46] T. Mosbach, H.-M. Katsch, and H. F. Döbele, Phys. Rev. Lett. **85**, 3420 (2000).
[47] T. Mosbach, V. Schulz-von der Gathen, and H. F. Döbele, Contrib. Plasma Phys. **42**, 650 (2002).
[48] P. Vankan, S. B. S. Heil, S. Mazouffre, R. Engeln, D. C. Schram, and H. F. Döbele, Rev. Sci. Instrum. **75**, 996 (2004).
[49] M. C. M. van de Sanden, G. M. Janssen, J. M. de Regt, D. C. Schram, J. A. M. van der Mullen, and B. van der Sijde, Rev. Sci. Instrum. **63**, 3369 (1992).
[50] S. Mazouffre, M. G. H. Boogaarts, I. S. J. Bakker, P. Vankan, R. Engeln, and D. C. Schram, Phys. Rev. E **64**, 016411 (2001).
[51] S. Mazouffre, P. Vankan, R. Engeln, and D. C. Schram, Phys. Plasmas **8**, 3824 (2001).
[52] H. Abgrall, E. Roueff, F. Launay, J.-Y. Roncin, and J.-L. Subtil, Astron. Astrophys. Suppl. Ser. **101**, 273 (1993).
[53] H. Abgrall, E. Roueff, F. Launay, J. Y. Roncin, and J. L. Subtil, J. Mol. Spectrosc. **157**, 512 (1993).
[54] S. Mazouffre, P. Vankan, R. Engeln, and D. C. Schram, Phys. Rev. E **64**, 066405 (2001).
[55] D. C. Schram, S. Mazouffre, R. Engeln, and M. C. M. van de Sanden, in *Atomic and Molecular Beams*, edited by R. Campargue (Springer, New York, 2001).
[56] P. Vankan, D. C. Schram, and R. Engeln, Chem. Phys. Lett. **400**, 196 (2004).
[57] P. Vankan, D. C. Schram, and R. Engeln, J. Chem. Phys. **121**, 9876 (2004).
[58] O. Gabriel, J. J. A. van den Dungen, W. M. Soliman, D. C. Schram, and R. Engeln, Chem. Phys. Lett. **451**, 204 (2008).
[59] P. Vankan, D. C. Schram, and R. Engeln, Plasma Sources Sci. Technol. **14**, 744 (2005).
[60] P. Vankan, R. Engeln, and D. C. Schram, Appl. Phys. Lett. **86**, 101501 (2005).
[61] R. Engeln, S. Mazouffre, P. Vankan, D. C. Schram, and N. Sadeghi, Plasma Sources Sci. Technol. **10**, 595 (2001).
[62] O. Gabriel, P. G. J. Colsters, D. C. Schram, and R. Engeln, Plasma Sources Sci. Technol. **17**, 015011 (2008).
[63] B. B. Hamel and D. R. Willis, Phys. Fluids **9**, 829 (1966).
[64] D. R. Flower and E. Roueff, J. Phys. B **32**, 3399 (1999).
[65] S. A. Wrathmall and D. R. Flower, J. Phys. B **39**, L249 (2006).
[66] E. M. Hollmann, A. Y. Pigarov, and K. Taylor, J. Nucl. Mater. **337-339**, 451 (2005).
[67] A. K. Rebrov, A. A. Morozov, M. Y. Plotnikov, N. I. Timoshenko, and A. V. Shishkin, J. Exp. Theor. Phys. **97**, 738 (2003).
[68] M. C. M. van de Sanden, J. M. de Regt, and D. C. Schram, Phys. Rev. E **47**, 2792 (1993).
[69] R. K. Grubbs and S. M. George, J. Vac. Sci. Technol. A **24**, 486 (2006).
[70] P. J. Chantry, J. Appl. Phys. **62**, 1141 (1987).
[71] J. P. Booth and N. Sadeghi, J. Appl. Phys. **70**, 611 (1991).